NATIONAL ADVISORY COMMITTEE FOR AERONAUTICS

TECHNICAL NOTE 3741

AN INVESTIGATION OF THE LOADS ON THE VERTICAL TAIL OF A JET-BOMBER AIRPLANE RESULTING FROM FLIGHT THROUGH ROUGH AIR

By Jack Funk and Richard H. Rhyne

Langley Aeronautical Laboratory
Langley Field, Va.

Washington

October 1956

NATIONAL ADVISORY COMMITTEE FOR AERONAUTICS

TECHNICAL NOTE 3741

AN INVESTIGATION OF THE LOADS ON THE VERTICAL TAIL OF A JET-BOMBER AIRPLANE RESULTING FROM FLIGHT THROUGH ROUGH AIR

By Jack Funk and Richard H. Rhyne

SUMMARY

Vertical-tail loads were measured in turbulent air on a four-engine jet bomber. The results showed large and regular load oscillations which were lightly damped. Comparison of experimental results with discrete-load calculations indicated that discrete-gust calculations underestimated the loads by 30 to 40 percent and gave no indication of the oscillatory characteristics or low damping. Calculations based on power spectral analysis, on the other hand, reflected the general frequency characteristics of the measured loads and gave a better estimate of the tail loads. The present results strongly indicate that discrete-gust calculations for gust loads on vertical tails may seriously underestimate the gust loads for airplanes having lightly damped lateral oscillations.

INTRODUCTION

Reference 1 suggests that the gust loads on the vertical-tail surface can be calculated satisfactorily by the sharp-edge-gust equation with no alleviation due to unsteady-lift effects or airplane motions. This recommendation was based on some early and limited flight tests of an XB-15 and an O-2H airplane in the late 1930's. Since these early tests, changes in airplane configuration and the large increase in speed have served to complicate the airplane responses to rough air. It was desirable, therefore, to reassess the problem of gust loads on the vertical-tail surface in order to determine whether the simplified relation of the sharp-edge-gust formula is still applicable.

A flight investigation was undertaken with a jet bomber in order to obtain experimental data on the magnitude and characteristics of the load on the vertical tail in rough air and to assess the significant factors affecting the tail loads. Flight tests were made at two center-of-gravity positions in order to provide a measure of the effects of changes in stability. The results of these test measurements are presented herein. Calculations of the loads on the vertical-tail surface due to

gusts were made as a supplement to the flight-load measurements in order to determine how accurately they could be predicted by existing procedures. Two types of calculations were considered: One was based on discrete-gust techniques, as suggested by reference 1; and the other, involving the statistical techniques of power spectral analysis, was based on continuous gust histories. The results of the calculations based on both methods are presented and compared with the flight-test measurements.

SYMBOLS

a lift-curve slope for wing, per radian

a_l lateral acceleration, g units

a_n normal acceleration, g units

b wing span, ft

C_n yawing-moment coefficient, N/qSb

$$C_{n_r} = \frac{\partial C_n}{\partial\left(\frac{rb}{2V}\right)}$$

$$C_{n_\beta} = \frac{\partial C_n}{\partial \beta}$$

C_Y lateral-force coefficient, Y/qS

$\left(C_Y\right)_{vt}$ lateral-force coefficient on vertical tail above strain measuring station

$$C_{Y_r} = \frac{\partial C_Y}{\partial\left(\frac{rb}{2V}\right)}$$

$$\left(C_{Y_r}\right)_{vt} = \frac{\partial\left(C_Y\right)_{vt}}{\partial\left(\frac{rb}{2V}\right)}$$

$C_{Y_\beta} = \frac{\partial C_Y}{\partial \beta}$

$\left(C_{Y_\beta}\right)_{vt} = \frac{\partial \left(C_Y\right)_{vt}}{\partial \beta}$

$\bar{c}$ mean aerodynamic chord of wing, ft

$\bar{c}_{vt}$ mean aerodynamic chord of vertical tail, ft

D_b differential operator with respect to s_b

d damping coefficient

g acceleration due to gravity, ft/sec^2

K_g gust factor (ref. 3)

K_X nondimensional radius of gyration about principal longitudinal axis, k_X/b

K_Z nondimensional radius of gyration about principal vertical axis, k_Z/b

K_{Zs} nondimensional radius of gyration about vertical stability axis, $\sqrt{K_Z^2 \cos^2\eta + K_X^2 \sin^2\eta}$

k_X radius of gyration about principal longitudinal axis, ft

k_Z radius of gyration about principal vertical axis, ft

k_2 variation of lift coefficient when penetrating a sharp-edge gust, expressed as a fraction of final lift

L scale of turbulence, ft

l_{vt} tail length (from center of gravity of airplane to 25 percent mean aerodynamic chord of vertical tail), ft

m mass of airplane, W/g, slugs

N	yawing moment on airplane, ft-lb
q	dynamic pressure, lb/sq ft
r	yawing angular velocity, radians/sec
S	wing area, sq ft
s_b	nondimensional time parameter based on span, $\frac{tV}{b}$
$T(\omega)$	frequency-response function
t	time, sec
U	true gust velocity, fps
U_{de}	derived gust velocity, fps (ref. 3)
V	true airspeed, fps
V_e	equivalent airspeed, fps
W	weight of airplane, lb
Y	lateral force on airplane, lb
Y_{vt}	aerodynamic load on 96-square-foot area of vertical tail above strain measuring station, lb (also used as subscript)
β	angle of slideslip, radians
η	angle between principal longitudinal axis of inertia and flight path, deg
μ_b	relative-density coefficient based on span, $m/\rho Sb$
μ_g	airplane mass ratio, $2W/\rho aS\bar{c}g$
ρ	density of air, slugs/cu ft
ρ_o	standard density of air at sea level, 0.002378 slug/cu ft
Φ_x	spectrum of longitudinal components of atmospheric turbulence
Φ_y	spectrum of lateral components of atmospheric turbulence

ψ angle of yaw, radians (also used as subscript)

Ω reduced frequency, ω/V, radians/ft

ω frequency, radians/sec

ω_0 undamped natural frequency, radians/sec

Dot over quantity denotes first derivative with respect to time.

METHOD AND TESTS

The method consisted of measuring the input-gust history and the load on the vertical tail during flight of the test airplane in rough air. Two measurements of the turbulence input were obtained. Derived gust velocities were obtained by using the normal acceleration to provide gust velocities for use in the discrete-gust calculations, and the rapid fluctuations of the airspeed were recorded to provide an input for the power spectral calculations. The loads on the vertical-tail surface were measured with calibrated electrical resistance strain gages mounted on the three spars of the vertical tail.

Two flights of approximately 40 miles each were made, one at a center-of-gravity position of 24.3 percent mean aerodynamic chord and one at a center-of-gravity position of 30.6 percent mean aerodynamic chord. The runs were made in clear rough air at an altitude of approximately 1,500 feet above the terrain and at an airspeed of approximately 390 knots. The pilot was instructed to use as little control motion as was consistent with safe flight.

AIRPLANE AND INSTRUMENTATION

The airplane used in this investigation was a jet-powered medium bomber. A line drawing of the airplane is shown in figure 1. The characteristics of the airplane pertinent to the present analysis are summarized in table I.

Vertical-tail loads were obtained from electrical wire resistance strain gages mounted on the three spars and from lateral-acceleration measurements at the vertical tail. The strain gages were installed approximately 14 inches above the horizontal tail as shown in figure 1 and were calibrated in a manner similar to that of reference 2. The various gage responses were not combined electrically but were recorded individually and combined numerically in the calibration equation. The

strain-gage outputs were recorded on an 18-channel oscillograph having elements with frequency responses that were flat to 60 cps or above. An NACA air-damped recording accelerometer was installed near the root of the vertical-tail surface (as shown in fig. 1) in order to obtain the inertia load. The accelerometer had a natural frequency of 14.7 cps and was damped to about 0.7 of critical.

In order to obtain data for evaluation of derived gust velocities, two accelerometers were installed near the front spar at approximately the nodal points of the wing fundamental bending mode (spanwise location approximately 245 inches from fuselage center line). The accelerometers were the strain-gage type having a natural frequency of about 12 cps and were oil-damped to 0.7 critical. Locating the accelerometers at the nodes eliminated the effect of the fundamental wing bending mode on the acceleration measurements. The two acceleration measurements were combined electrically to eliminate the effects of roll and were recorded on a galvanometer with a natural frequency of about 12 cps.

In addition to the measurement of turbulence obtained from the vertical acceleration, turbulence measurements were obtained from the recorded airspeed fluctuations. Inasmuch as the airplane is longitudinally insensitive to turbulence at the higher frequencies, the airspeed fluctuations at these frequencies are a direct measure of the turbulence. For the present investigation, it was estimated that this condition would apply for the range of frequencies above 1/4 cps. The airspeed fluctuations were measured with a standard NACA airspeed-altitude recorder which had a natural frequency of about 100 cps. The pitot-static head was located on a boom about 6 feet forward of the nose to minimize errors in static pressure. The pitot lines were made as short as possible, balanced, and damped with orifices to provide a frequency response which was shown by calibration to be flat to about 10 cps.

Measurements were made of the fuselage flexibility by using two yaw-attitude recorders, one mounted at the center of gravity of the airplane and the other mounted in the tail. Differences in the yaw-angle reading of the two recorders gave the change in angle of sideslip of the tail due to fuselage flexibility.

In addition to the above data, measurements were obtained of the control-surface positions, rolling velocity, pitch attitude, and yaw angle.

EVALUATION OF DATA AND RESULTS

As an indication of the general characteristics of the records, short sections of some of the pertinent quantities measured are shown

in figure 2. The methods used in the evaluation of these records can be conveniently separated into two parts: one pertaining to the discrete-gust procedure and the other involving power spectra as will be described.

As a starting point for the discrete-gust and spectral evaluations, 300-second sections of the pertinent records were read at 0.1-second intervals along the time history. From the 0.1-second-interval readings of strain and lateral acceleration, the vertical-tail airload was determined from the relation

Vertical-tail airload = Structural shear load + Inertia load

where the inertia load is the product of the mass of the structure extending above the strain-gage station and its measured lateral acceleration. The evaluation of the structural shear load was made for incremental loadings from the trim load which was taken as the mean load for each test run. The shear load was determined from the shear strain gages located on the three spars. Static calibration of the shear gages indicated that the shear readings were affected by the bending moment in the structure so that the total shear at the root is given by the relation

$$\text{Structural shear load} = A\delta_{s1} + B\delta_{s2} + C\delta_{s3} + D\delta_{b1} + E\delta_{b2} + F\delta_{b3}$$

where δ_{s1}, δ_{s2}, and δ_{s3} are the shear-gage responses and δ_{b1}, δ_{b2}, and δ_{b3} are the bending-moment-gage responses. The evaluation of several of the larger loads indicated that the contribution of the bending moment would add less than 1.5 percent to the shear load; therefore, the effect of the bending moment was neglected in the shear evaluations.

Flexibility

Bending of the fuselage under the load on the vertical-tail surface causes a small change in the angle of sideslip at the tail which acts to reduce the load on the vertical tail. This change in sideslip angle due to fuselage flexibility was evaluated by using the two yaw-attitude recorders installed at the center of gravity and at the tail of the airplane. Inspection of the yaw-attitude record at the tail indicated that the change in sideslip due to the fundamental fuselage mode was so small that it was within the reading error of the records. Thus, it appears that the effect of fuselage flexibility, if any, will be that due to "static" bending under the tail load.

As a preliminary check on the magnitude of the effects of the static fuselage bending on the tail loads, incremental changes in yaw attitude corresponding to the change in vertical-tail airload from maximum to

minimum or minimum to maximum (such as shown by the solid circles in fig. 2) were evaluated from both the center-of-gravity and tail yaw-attitude records. The difference between the incremental change at the center of gravity and at the tail was taken as an incremental angle of sideslip at the tail due to fuselage flexibility. The associated change in load due to fuselage flexibility was then calculated from the conventional lift equation by use of the incremental sideslip data. The results of this check indicated that, on the average, fuselage flexibility reduced the loads on the vertical-tail surface by about 10 percent.

Discrete-Gust Analysis

Peak vertical-tail loads.- The frequency distributions of the peak tail loads were evaluated from the time-history plot of the 0.1-second readings of vertical-tail airload as follows: The mean load was first determined from the 0.1-second readings. Then the values of the peak positive and negative load increments between successive crossings of the mean load line were tabulated into 100-pound class intervals. The distributions obtained for the two center-of-gravity positions are given in table II.

From the tabulated data, the average flight miles required to exceed given values of load increment $M(\Delta Y_{vt})$ were determined by the following relation:

$$M(\Delta Y_{vt}) = \frac{\text{Total miles}}{N(\Delta Y_{vt})}$$

where $N(\Delta Y_{vt})$ is the number of peak values exceeding a given value of load increment. The results obtained for the two test center-of-gravity positions are shown in figure 3 and represent the basic description of the load history. It should be noted that these data include the effects of turbulence variation between test runs.

Derived gust velocity.- Distributions of derived gust velocity were calculated from the peak nodal accelerations according to the derived-gust-velocity formula from reference 3:

$$a_{n_{max}} = \frac{a\rho_o S V_e U_{de}}{2W} K_g$$

where

$a_{n_{max}}$ airplane maximum nondimensional normal acceleration in g units

The nodal accelerations were evaluated from the steady-flight position of the acceleration trace for the largest peak between consecutive crossings of the steady-flight trace position. Derived gust velocities were then calculated from these peak readings and are tabulated into frequency distributions in table III. These distributions were used to determine the average flight miles required to exceed a given gust velocity in a manner similar to that used for the vertical-tail loads, and the results obtained are plotted in figure 4.

Power Spectral Analysis

Vertical-tail load spectra.- In addition to the discrete-gust analysis, power spectra of the gust loads on the vertical-tail surface were obtained to show the frequency content of the load histories and to be compared with the theoretical calculations. The load spectra were calculated by the procedure suggested by Tukey in reference 4 and reviewed in reference 5. Initially, calculations were made to cover the range from 0 to 5 cps and were based on a 3,000-point sample taken at 0.1-second intervals along the time history. Autocorrelation functions of 40 lags were made from which 40 power estimates were obtained over the frequency range of 0 to 5 cps. These results are shown in figures 5(a) and 5(b) for the tests at center-of-gravity positions of 24.3 and 30.6 percent mean aerodynamic chord, respectively, and are designated by the term "wide filter." (This numerical calculation can be viewed as equivalent to scanning the true spectrum with a roughly triangular filter having a 1/2-cps base width.)

Because of the peakedness of the measured spectra, a second analysis was made to determine more precisely the shape in the vicinity of peak power. The second spectra were obtained from 600-point samples taken at 1/2-second intervals along the time histories. (Only every fifth reading of the original data was used.) Autocorrelation functions of 60 lags were calculated from which 60 power estimates covering the frequency range of 0 to 1 cps were obtained. (If 60 power estimates had been obtained for the frequency range of 0 to 1 cps for all 3,000 readings at a 0.1-second interval, 300 lags for the autocorrelation function would have been required. The procedure used permitted a more practical calculation without any appreciable loss in reliability for the estimates over the desired range.) The effective filter width for this analysis is about 1/15 cps. The results are also shown in figures 5(a) and 5(b) and are designated by the term "narrow filter."

Because of the limited record lengths, individual power spectral estimates are not too reliable - roughly, ± 30 percent of the values shown in figure 5. The reliability of the overall power for each case is, of course, considerably greater, with the root-mean-square values estimated to be reliable to about ± 10 percent of the value obtained.

Gust spectra.- In order to calculate the spectra of the vertical-tail load for comparison with the spectra of the measured load, it was necessary to obtain a measure of the spectra of the lateral gust velocity. Although no direct measurements of the lateral-gust-velocity spectra were made, references 6 and 7 suggest that a satisfactory measure may be obtained from the power spectra of the longitudinal gust velocity on the assumption that atmospheric turbulence is isotropic. The longitudinal-gust-velocity spectra were, therefore, evaluated from 0.1-second-interval readings of the airspeed records.

The power spectra of the airspeed fluctuations were characterized by a very large peak in power at the low frequencies. The effects of such large peaks is to introduce some errors into the spectral analysis at the higher frequencies. In such cases, it is frequently helpful, as pointed out in reference 8, to reduce the power at the peaks by properly filtering the original data. This procedure is sometimes referred to as "prewhitening."

The power at the low frequencies was reduced in amplitude before the spectral analysis was made by applying a high-pass filter to the data. The filter consisted of subtracting a moving average over a 5-second interval from the time history of airspeed. This technique is discussed in reference 8, in which it is shown that this procedure alters the power spectra by the factor

$$\left(1 - \frac{\sin \frac{\omega T}{2}}{\frac{\omega T}{2}}\right)^2$$

where T is the total time interval over which the moving average is taken. For T of 5 seconds, almost all the power below 0.2 cps is removed. The spectra obtained from the filtered data were multiplied by the reciprocal of the foregoing filter in order to compensate for the initial filtering. The resulting airspeed spectra are presented in figure 6. As a simple measure of the relative intensity of the turbulence for the two test runs, the root-mean-square values of the spectra above 0.2 cps are given in figure 6. The power below 0.2 cps was not included because little power appears in the load spectra below 0.2 cps.

CALCULATIONS

Discrete-Gust Calculations

The simplest approach for calculating the load on the vertical tail for a discrete gust is to compute the load resulting from a steady-state angle-of-sideslip change due to the gust. This procedure has been suggested for calculating gust load on a vertical-tail surface in reference 1

and with some modification is the basis for most current design procedures. The load on the vertical tail is obtained by substituting U_{de}/V for the angle of sideslip due to the gusts so that

$$Y_{vt} = \frac{1}{2} \rho_o \left(C_{Y_\beta}\right)_{vt} S V_e U_{de} \tag{1}$$

where Y_{vt} is the load on the 96-square-foot area above the strain measuring station, and $\left(C_{Y_\beta}\right)_{vt}$ is the slope of the lateral-force coefficient for the 96-square-foot area. By use of the preceding equation, the average flight miles to exceed given values of peak vertical-tail load were computed from the faired distributions of the derived gust velocity of figure 4. The values obtained are presented in figure 3 as the curves labeled "discrete calculations." These calculated loads are for the 96-square-foot area above the strain measuring station so that they can be compared directly with the measured loads. The value of $\left(C_{Y_\beta}\right)_{vt}$ used for the calculations was obtained from the flight-test results of reference 9.

Spectral Calculations

The basic relation between the power spectrum of the response of a linear system to a random disturbance and the spectrum of the disturbance is given as (see ref. 5)

$$\Phi_o(\omega) = \left|T(\omega)\right|^2 \Phi_i(\omega) \tag{2}$$

where

$\Phi_o(\omega)$ power spectrum of response or output

$T(\omega)$ frequency-response function

$\Phi_i(\omega)$ power spectrum of disturbance or input

and where bars designate the absolute value of the complex quantity.

The application of this relation to the calculation of the vertical-tail load requires the determination of (1) the frequency-response function $T(\omega)$ for the load on the vertical tail due to unit sinusoidal lateral gusts and (2) the lateral-gust-velocity spectrum. The methods used in determining these two functions are considered in the succeeding section.

Frequency-response function.- For the present analysis, the following assumptions were made: (1) the airplane did not roll, (2) the

vertical-tail loads were due to side gusts only, and (3) the pilot had little effect on the loads. Inasmuch as the flight records indicated very small roll angles due to the action of the gusts, the restriction to the no-roll condition appeared justified. The small roll angles $\left(\text{about } 1\frac{1}{2}^{\circ}\right)$ also indicated that the asymmetrical component of the vertical gust velocity over the wing, which might give rise to sideslip motion and to load on the vertical tail, had little effect in the present case.

Lag in lift was taken into consideration by applying the gust penetration function $k_2(s)$ for a Mach number of 0.6 (from ref. 10) on the assumption that the greater parts of the side-force and yawing-moment coefficients come from the vertical-tail surface. This procedure is thought to give a satisfactory approximation to the effects of lag in lift. (Actually, the lag in lift was found to have very little effect on the calculated load spectra, the effect being a further attenuation of the spectra at the higher frequencies. However, the lag in lift did significantly affect the second moment of the spectra, which was needed in subsequent calculations of peak load.) From the preceding considerations, the load on the vertical tail due to side gusts is given by the expression

$$Y_{vt}(t) = qS\left(C_{Y_\beta}\right)_{vt}\beta(t) + qS\left(C_{Y_r}\right)_{vt}\frac{b}{2V}\dot{\psi}(t) - \frac{qS\left(C_{Y_\beta}\right)_{vt}}{V}\int_0^t k_2(t - t_1)\frac{dU(t_1)}{dt_1}dt_1 \qquad (3)$$

The first term on the right-hand side of equation (3) is the load due to sideslip, the second term is the load due to yawing velocity, and the last term is the load due to the gust. The lag-in-lift function due to gust penetration k_2 is usually given in terms of airfoil chord length. It was changed to the time argument by the relation $s = \frac{tV}{\bar{c}_{vt}}$.

The frequency-response function for vertical-tail load $T_{Y_{vt}}(\omega)$ is obtained by substituting

$$U(t_1) = U(\omega)e^{i\omega t_1}$$

$$\psi(t) = \psi(\omega)e^{i\omega t}$$

$$\beta(t) = \beta(\omega)e^{i\omega t}$$

$$Y_{vt}(t) = Y_{vt}(\omega)e^{i\omega t}$$

into equation (3) and solving for $\frac{Y_{vt}(\omega)}{U(\omega)}$. The result is

$$\frac{Y_{vt}(\omega)}{U(\omega)} = qS\left(C_{Y_\beta}\right)_{vt}\frac{\beta(\omega)}{U(\omega)} + i\omega qS\left(C_{Y_r}\right)_{vt}\frac{b}{2V}\frac{\psi(\omega)}{U(\omega)} - \frac{qS\left(C_{Y_\beta}\right)_{vt}}{V}\left[P(\omega) + iQ(\omega)\right] \tag{4}$$

which may be written as

$$T_{Yvt}(\omega) = qS\left(C_{Y_\beta}\right)_{vt}T_\beta(\omega) + i\omega qS\left(C_{Y_r}\right)_{vt}\frac{b}{2V}T_\psi(\omega) - \frac{qS\left(C_{Y_\beta}\right)_{vt}}{V}\left[P(\omega) + iQ(\omega)\right] \tag{4a}$$

where

$$P(\omega) + iQ(\omega) = i\omega\int_0^\infty k_2(t)e^{-i\omega t}dt$$

$$T_\beta(\omega) = \frac{\beta(\omega)}{U(\omega)}$$

$$T_\psi(\omega) = \frac{\psi(\omega)}{U(\omega)}$$

$$T_{Yvt}(\omega) = \frac{Y_{vt}(\omega)}{U(\omega)}$$

The sideslip frequency-response function $T_\beta(\omega)$ and yaw frequency-response function $T_\psi(\omega)$ may be determined from the conventional lateral equations of motion for two degrees of freedom such as are given in reference 11. If the conventional stability axes shown in figure 7 are used, these equations become:

Sideslip:

$$\left(2\mu_b D_b - C_{Y_\beta}\right)\beta + \left(2\mu_b D_b - \tfrac{1}{2}C_{Y_r}D_b\right)\psi =$$

$$-\frac{C_{Y_\beta}}{V}\int_0^{s_b} k_2\left(s_b - s_{b1}\right)\frac{dU\left(s_{b1}\right)}{ds_{b1}}ds_{b1} \tag{5}$$

Yaw:

$$-C_{n_\beta}\beta + \left(2\mu_b K_{Zs}^2 D_b^2 - \frac{1}{2} C_{n_r} D_b\right)\psi =$$

$$-\frac{C_{n_\beta}}{V}\int_0^{s_b} k_2\left(s_b - s_{b1}\right)\frac{dU\left(s_{b1}\right)}{ds_{b1}}\,ds_{b1} \tag{6}$$

In equations (5) and (6), the operator D_b has been used to denote the differential $\frac{d}{ds_b}$ where s_b is the nondimensional time parameter $\frac{tV}{b}$. The lag-in-lift function k_2 which is usually expressed in terms of mean aerodynamic chord is converted to the new variable by the relation $b = 9.3\bar{c}_{vt}$. The two equations are solved simultaneously for $T_\psi(\omega)$ and $T_\beta(\omega)$. The results obtained are given by

$$T_\psi(\omega) = -\frac{C_{n_\beta}}{2\mu_b K_{Zs}^2 V}\frac{P(\omega) + iQ(\omega)}{-\frac{b^2}{V^2}\omega^2 + A\frac{b}{V}i\omega + B} \tag{7}$$

$$T_\beta(\omega) = \frac{-\frac{1}{V}\left(\frac{C_{Y_\beta} b}{2\mu_b V}i\omega - B\right)\left[P(\omega) + iQ(\omega)\right]}{-\frac{b^2}{V^2}\omega^2 + A\frac{b}{V}i\omega + B} \tag{8}$$

where

$$A = -\frac{C_{n_r}}{4\mu_b K_{Zs}^2} - \frac{C_{Y_\beta}}{2\mu_b}$$

$$B = \frac{C_{n_\beta}}{2\mu_b K_{Zs}^2} + \frac{C_{n_r} C_{Y_\beta}}{8\mu_b^2 K_{Zs}^2} - \frac{C_{n_\beta} C_{Y_r}}{8\mu_b^2 K_{Zs}^2}$$

Substituting equations (7) and (8) into equation (4a) gives the frequency-response function for the loads on the vertical tail as

$$T_{Yvt}(\omega) = -\frac{qS\left(C_{Y_\beta}\right)_{vt}\left[-\omega^2 + \frac{VC_{n_\beta}\left(C_{Y_r}\right)_{vt}}{4\mu_b K_{Z_s}{}^2 b\left(C_{Y_\beta}\right)_{vt}} i\omega - \frac{VC_{n_r}}{4\mu_b K_{Z_s}{}^2 b} i\omega\right]\left[P(\omega) + iQ(\omega)\right]}{V\left(\omega_o{}^2 - \omega^2 + 2di\omega\right)} \tag{9}$$

where

$$2d = -\frac{VC_{n_r}}{4\mu_b K_{Z_s}{}^2 b} - \frac{VC_{Y_\beta}}{2\mu_b b}$$

$$\omega_o{}^2 = \frac{V^2 C_{n_\beta}}{2\mu_b K_{Z_s}{}^2 b^2} + \frac{V^2 C_{n_r} C_{Y_\beta}}{8\mu_b{}^2 K_{Z_s}{}^2 b^2} - \frac{V^2 C_{n_\beta} C_{Y_r}}{8\mu_b{}^2 K_{Z_s}{}^2 b^2}$$

Estimation of stability derivatives.- The stability derivatives necessary for calculating the transfer functions were estimated in the following manner: The coefficient $\left(C_{Y_\beta}\right)_{vt}$ for the 96 square feet of vertical-tail surface above the strain gages was obtained from the tests of reference 9. The coefficient C_{Y_β} for the whole airplane was estimated by using the load measurements on the vertical tail and the lateral accelerometer at the center of gravity. The ratio of the total side load obtained from the lateral accelerometer to the measured load on the vertical tail was determined. Multiplying this ratio by $\left(C_{Y_\beta}\right)_{vt}$ gave C_{Y_β} for the whole airplane. This method assumes that the effect of flexibility on the fuselage aerodynamics is the same as for the vertical tail. The value of C_{Y_β} obtained in this manner is thought to be compensated for the effects of steady-state flexibility. On the assumption that the yawing moment is produced by the forces on the vertical tail, C_{n_β} was estimated from

$$C_{n_\beta} = -C_{Y_\beta}{}' \frac{l_{vt}}{b}$$

where $C_{Y_\beta}{}'$ refers to the derivative for the complete tail area (127.8 square feet) and was obtained from $\left(C_{Y_\beta}\right)_{vt}$ on the basis that the derivatives were proportional to the ratio of the areas.

The values for C_{Y_r} and C_{n_r} were estimated from the relation

$$C_{Y_r} = -C_{Y_\beta} \cdot \frac{l_{vt}}{b/2}$$

$$C_{n_r} = 2C_{Y_\beta} \cdot \frac{l_{vt}^2}{b^2}$$

$$\left(C_{Y_r}\right)_{vt} = -\left(C_{Y_\beta}\right)_{vt} \frac{l_{vt}}{b/2}$$

where the derivative $\left(C_{Y_r}\right)_{vt}$ refers to the 96 square feet of area above the strain-gage station. The stability derivatives estimated in the above manner are tabulated in table IV.

By use of the stability derivatives in table IV and equation (9), the frequency-response functions for the vertical-tail load were calculated and the amplitude squared of the frequency responses are shown in figure 8 for the two center-of-gravity positions.

Input-gust spectra.- The spectra of the input-gust velocity were based on the spectra of airspeed fluctuations. However, as indicated previously, the airspeed fluctuations measure the longitudinal component of the turbulence, whereas the vertical-tail loads are essentially the result of the side or lateral turbulence. On the assumption that atmospheric turbulence is isotropic, these two spectra are related. The spectrum of the lateral component of atmospheric turbulence, as indicated in reference 12, appears to be approximated very well by the following expression:

$$\Phi_y(\Omega) = \sigma_U^2 \frac{L}{\pi} \frac{1 + 3\Omega^2L^2}{\left(1 + \Omega^2L^2\right)^2} \tag{10}$$

where

σ_U root-mean-square gust velocity

The expression for the spectrum of the longitudinal component for isotropic turbulence corresponding to equation (10) is given by

$$\Phi_x(\Omega) = \sigma_U^2 \frac{2L}{\pi} \frac{1}{1 + \Omega^2L^2} \tag{11}$$

(See appendix of ref. 7.) If equations (10) and (11) are compared, it can be seen that the ratio of $\Phi_y(\Omega)$ to $\Phi_x(\Omega)$ depends upon the value of L and varies with the value of Ω. Reference 12, together with an

examination of the airspeed spectra of figure 6, suggests that L is of the order of 1,000 feet or greater for the turbulence encountered. For L of 1,000 feet and greater, $\Phi_y(\Omega)$ is approximately 1.5 times the value of $\Phi_x(\Omega)$ for values of Ω greater than about 0.002, which in the present case corresponds to frequencies above 0.2 cps. The input-gust spectra for the calculation of the vertical-tail loads were accordingly obtained by multiplying the longitudinal spectra (fig. 6), obtained from the airspeed measurements, by 1.5.

The gust-load spectra for the vertical-tail surface were calculated by multiplying the input spectra discussed previously by the frequency-response functions (fig. 8) and are also shown in figure 5 for comparison with the measured load spectra.

Effect of errors in stability derivatives.- In order to evaluate the reliability of the calculation, the effects of errors in the stability derivatives on the calculations were considered. Unfortunately, there is no exact way to check the reliability of the stability derivatives. However, experience suggests that C_{Y_β} and C_{n_β} are reliable to ±10 percent and that C_{n_r} is reliable to ±15 percent. The other stability derivatives have a much smaller effect on the results, and errors in these derivatives are of little importance.

Calculations were made to show the effect of errors in C_{Y_β}, C_{n_β}, and C_{n_r} on the root-mean-square load. Each of these derivatives was individually reduced by 10 percent and a new value of the root-mean-square load was calculated by use of the gust-input spectra of figure 6 and equations (2) and (9). The results showed that reducing both C_{Y_β} and $\left(C_{Y_\beta}\right)_{vt}$ by 10 percent reduced the root-mean-square tail load about 8 percent; a 10-percent reduction in C_{n_β} reduced the root-mean-square tail load less than 1 percent, and a 10-percent reduction in C_{n_r} increased the root-mean-square tail load by 4 percent. Therefore, the overall uncertainties in the stability derivatives are roughly estimated to yield uncertainties in the calculated root-mean-square loads of the order of ±10 to ±15 percent.

Calculation of Peak-Load Distribution

One of the principal objects of gust-load calculations is to estimate the magnitude and frequency of load peaks for use in design. If atmospheric turbulence is considered to be a simple Gaussian disturbance, the average number of peak loads per second exceeding a given value is,

as indicated in reference 12, given by

$$N(Y_{vt}) = \frac{1}{2\pi}\left[\frac{\int_0^\infty \omega^2\Phi(\omega)d\omega}{\int_0^\infty \Phi(\omega)d\omega}\right]^{1/2} e^{-Y_{vt}^2/2\sigma_{Yvt}^2} \tag{12}$$

where σ_{Yvt} is the root-mean-square tail load and $\Phi(\omega)$ is the power spectrum of the tail load.

A simple evaluation of equation (12) for the calculated load spectra of figure 5 indicated that the shape of the calculated curve $N(Y_{vt})$ did not conform to the measurements. The character of the difference was a less rapid increase in the calculated load with increasing flight miles than that for the measured load. This characteristic difference between flight measurements and calculations based on Gaussian theory has been noted in other studies and is discussed in reference 12 in which it is attributed to a lack of homogeneity in the intensity of atmospheric turbulence. Reference 12 indicates that flight-test data on peak gust loads can generally be synthesized by a combination of Gaussian turbulence disturbances which vary in intensity but which have the same spectral form. For these conditions, the number of peak loads exceeding a given value of Y_{vt} is given by

$$N(Y_{vt}) = \frac{1}{2\pi}\left[\frac{\int_0^\infty \omega^2\Phi(\omega)d\omega}{\int_0^\infty \Phi(\omega)d\omega}\right]^{1/2} \sum_{n=1}^{m} e^{-Y_{vt}^2/2\sigma_n^2} \tag{13}$$

where σ_n is the root-mean-square load for the individual Gaussian components.

This model was applied by determining the root-mean-square gust velocity for 30 segments of equal length for the present test data. The root-mean-square loads σ_n were then taken proportional to the gust intensities for the corresponding segments. Equation (13) was then evaluated for the data of both center-of-gravity positions and the results obtained are shown in figure 3.

DISCUSSION

General Characteristics of Measured Load

The general characteristics of the loads on the vertical tail in rough air are indicated by the sample load history shown in figure 2. The load history in rough air exhibits a continuous oscillation at a frequency of about 0.4 cps with varying amplitude. This load time history is characteristic of a lightly damped system responding to an irregular but continuous exciting force. Comparison of the record samples shown in figure 2 indicates that both the loads and the shear strains closely follow the yawing oscillation of the airplane. Comparison of the load time history with the normal-acceleration record gives the impression that there is little or no correlation between these two quantities. The almost periodic and lightly damped characteristic of the loads on the vertical-tail surface indicated by the sample records is also noted in the power spectra of the vertical-tail loads for the whole test run shown in figure 5. The large power peak at a frequency of 0.36 cps is indicative of the response of lightly damped systems.

Effect of Center-of-Gravity Position

The distribution of measured peak loads on the vertical-tail surface for the two center-of-gravity positions shown in figure 3 cannot be directly compared in order to obtain the effect of center-of-gravity movement because the data are uncorrected for changes in turbulence intensity between test runs. Interpreting the data for the effects of the center-of-gravity position is further complicated by a difference in moment of inertia for the two tests due to the fuel load. The gust-velocity spectra shown in figure 6 indicate that the turbulence intensity for the tests at the forward center-of-gravity position was greater than the turbulence intensity for the rearward center-of-gravity position by a factor of about 1.13. The measured root-mean-square load for the forward center-of-gravity position is greater than that for the rearward center-of-gravity position by a factor of 1.08. Thus, a 5-percent increase in loads with rearward movement of the center of gravity and the simultaneous decrease in moment of inertia is indicated.

If the calculated results shown in figure 5 were adjusted for the differences in turbulence intensity, the results would yield roughly the same root-mean-square load for both test conditions. Check calculations showed that the decrease in moment of inertia would decrease the calculated root-mean-square load only about 1 percent and that the rearward movement of the center of gravity (shorter tail length) would increase the root-mean-square load only about 2 percent.

Taken individually, the effect on the calculations of either the center-of-gravity movement or the moment-of-inertia change was very small, and the combined effects of both would not be expected to cause a 5-percent difference in the root-mean-square values. In view of the accuracy of both the test results and the calculations, the indicated discrepancy of about 5 percent between test results and calculations is not too surprising. In any case, the effects on the loads in the present tests of the center-of-gravity movement and moment-of-inertia change appear very small.

Comparison of Calculated and Measured Loads

Figure 3 shows that the peak-load distributions on the vertical tail, calculated by the discrete-gust method, are considerably lower than the measured distributions. The load that would be exceeded on the average once in 35 flight miles was taken to be 3,600 pounds. The calculated peak loads by the discrete-gust method for this same flight distance are 2,150 pounds for the forward center-of-gravity position or 0.60 of the measured load and 2,550 pounds for the rearward center-of-gravity position or 0.71 of the measured load. It is also to be noted that the shapes of the calculated peak-load distributions based on discrete gust are considerably different from the measured distributions. For these test conditions, apparently the discrete-gust method of calculating gust loads seriously underestimates the gust loads on the vertical-tail surface.

The peak-load distributions calculated from the power spectra by the method of reference 12, and shown in figure 3, are in better agreement with the measured results than the discrete-gust calculations, both in amplitude and in shape. The loads that would be exceeded on the average once in 35 miles of flight are calculated to be 3,300 pounds for the forward center-of-gravity position and 2,700 pounds for the rearward center-of-gravity position. These values are, respectively, 0.92 and 0.75 of the measured loads. The calculations for the forward center-of-gravity positions are in good agreement with the measured values, whereas the results for the rearward center-of-gravity position are not nearly so good.

The difference between the spectral-calculation results and measured distributions is primarily due to the fact that the values of the root-mean-square load obtained from the calculated spectra were lower than the measured root-mean-square-load values. For the forward center of gravity where the calculated root-mean-square load was 91 percent of the measured root-mean-square load, good agreement was obtained between the calculated and the measured distributions. For the rearward center-of-gravity position, however, where the calculated root-mean-square load was only 85 percent of the measured root-mean-square load, the agreement between the calculated and the measured peak-load distributions was not so good. The 15-percent difference in root-mean-square load for the calculated and the measured spectra for the rearward center-of-gravity position appears to be too large for satisfactorily estimating the peak-load distributions.

It is evident that estimates of the distributions of peak load based on power spectra are better than the discrete-gust estimates. For the present analysis, estimates of the peaks based on the spectral techniques still underestimate the loads by as much as 25 percent. This fact is not too surprising, however, in view of the uncertainties in the gust input and in the estimates of the stability derivatives.

CONCLUSIONS

Results of flight tests of a jet-bomber airplane flown in turbulent air at center-of-gravity positions of 24.3 percent and 30.6 percent mean aerodynamic chord indicated that turbulence excited lightly damped lateral oscillations of the airplane. The loads on the vertical tail resulting from the lateral oscillations were considerably greater than the loads predicted by discrete-gust calculations. The loads predicted by discrete-gust calculations were 0.60 and 0.71 of the loads resulting from the lateral oscillations for the test runs at forward and rearward center-of-gravity positions, respectively.

Calculation of the load power spectra indicated the oscillatory nature and low damping of the loads on the vertical-tail surface. The root-mean-square loads from the spectral calculation were in good agreement with the measured values, being 0.91 and 0.85 of the measured root-mean-square load. The underestimation of the values of the root-mean-square load by the spectral calculations appears to be within the estimated error for the airplane stability derivatives and gust spectra.

Calculation of the peak-load distributions from the power spectra by the method used in NACA Technical Note 3540 was in fair agreement with the measured peak-load distributions. The errors in the calculated peak-load distributions appeared to be primarily due to the underestimation of the values of the root-mean-square load by the calculated power spectra.

Langley Aeronautical Laboratory,
National Advisory Committee for Aeronautics,
Langley Field, Va., May 8, 1956.

REFERENCES

1. Donely, Philip: Summary of Information Relating to Gust Loads on Airplanes. NACA Rep. 997, 1950. (Supersedes NACA TN 1976.)

2. Skopinski, T. H., Aiken, William S., Jr., and Huston, Wilber B.: Calibration of Strain-Gage Installations in Aircraft Structures for the Measurement of Flight Loads. NACA Rep. 1178, 1954. (Supersedes NACA TN 2993.)

3. Pratt, Kermit G., and Walker, Walter G.: A Revised Gust-Load Formula and a Re-Evaluation of V-G Data Taken on Civil Transport Airplanes From 1933 to 1950. NACA Rep. 1206, 1954. (Supersedes NACA TN's 2964 by Kermit G. Pratt and 3041 by Walter G. Walker.)

4. Tukey, John W.: The Sampling Theory of Power Spectrum Estimates. Symposium on Applications of Autocorrelation Analysis to Physical Problems (Woods Hole, Mass.), June 13-14, 1949, pp. 47-67. (Sponsored by ONR, Dept. Navy.)

5. Press, Harry, and Houbolt, John C.: Some Applications of Generalized Harmonic Analysis to Gust Loads on Airplanes. Jour. Aero. Sci., vol. 22, no. 1, Jan. 1955, pp. 17-26, 60.

6. Chilton, Robert G.: Some Measurements of Atmospheric Turbulence Obtained From Flow-Direction Vanes Mounted on an Airplane. NACA TN 3313, 1954.

7. Liepmann, H. W.: On the Application of Statistical Concepts to the Buffeting Problem. Jour. Aero. Sci., vol. 19, no. 12, Dec. 1952, pp. 793-800, 822.

8. Walls, James H., Houbolt, John C., and Press, Harry: Some Measurements and Power Spectra of Runway Roughness. NACA TN 3305, 1954.

9. Cooney, T. V.: The Vertical-Tail Loads Measured During a Flight Investigation on a Jet-Powered Bomber Airplane. NACA RM L52G21, 1953.

10. Mazelsky, Bernard, and Drischler, Joseph A.: Numerical Determination of Indicial Lift and Moment Functions for a Two-Dimensional Sinking and Pitching Airfoil at Mach Numbers 0.5 and 0.6. NACA TN 2739, 1952.

11. Bird, John D.: Some Calculations of the Lateral Response of Two Airplanes to Atmospheric Turbulence With Relation to the Lateral Snaking Problem. NACA TN 3425, 1955. (Supersedes NACA RM L50F26a.)

12. Press, Harry, and Meadows, May T.: A Reevaluation of Gust-Load Statistics for Applications in Spectral Calculations. NACA TN 3540, 1955.

TABLE I

AIRPLANE CHARACTERISTICS

General:	
Gross wing area, sq ft	1,175
Mean aerodynamic chord, ft	14.01
Aspect ratio	6.75
Lift-curve slope for wing, per radian (computed from $6A/(A+2)$ where A is aspect ratio)	4.63
Wing span, ft	89.04
Lift-curve slope for vertical tail per radian (ref. 9)	1.85
Vertical-tail geometry:	
Total area of vertical tail, sq ft	127.8
Vertical-tail area extending above horizontal tail, sq ft	109.4
Vertical-tail area above strain-gage location, sq ft	96.0
Mean aerodynamic chord, ft	9.37
Location of strain-gage bridges above horizontal tail, in.	13.6
Rudder and tab area, sq ft	28
Aspect ratio	1.43
Span extending above horizontal tail, in.	150
Chord at attachment to horizontal tail, in.	145
Chord at tip, in.	64
Fin offset, deg	0
Weight of vertical-tail structure extending above strain-gage bridges, lb	360
Rearward center-of-gravity position:	
Center-of-gravity position, percent mean aerodynamic chord	30.6
Airplane weight, lb	60,200
Average equivalent airspeed, ft/sec	662
Airplane mass ratio, $2W/\rho aS\bar{c}g$	22.0
Gust factor, K_g (ref. 3)	0.708
Air density, ρ, slugs/cu ft	0.002235
Moment of inertia about Z-axis, slug-ft^2	699,000
Tail length, ft (from center of gravity to quarter chord of vertical tail)	32.1
Forward center-of-gravity position:	
Center-of-gravity position, percent mean aerodynamic chord	24.3
Airplane weight, lb	61,200
Average equivalent airspeed, ft/sec	652
Airplane mass ratio, $2W/\rho aS\bar{c}g$	21.3
Gust factor, K_g (ref. 3)	0.705
Air density, ρ, slugs/cu ft	0.002337
Moment of inertia about Z-axis, slug-ft^2	735,000
Tail length, ft (from center of gravity to quarter chord of vertical tail)	32.9

TABLE II

FREQUENCY DISTRIBUTION OF PEAK AERODYNAMIC LOAD ON THE VERTICAL TAIL IN ROUGH AIR

Center-of-gravity position, 30.6, percent mean aerodynamic chord			Center-of-gravity position, 24.3, percent mean aerodynamic chord		
Class interval, lb	Frequency		Class interval, lb	Frequency	
	Right	Left		Right	Left
0	40	19	0	34	32
100	31	17	100	26	14
200	10	20	200	19	25
300	10	18	300	16	23
400	6	16	400	11	17
500	10	7	500	10	13
600	11	11	600	6	6
700	10	21	700	12	16
800	12	6	800	10	10
900	7	12	900	11	11
1,000	14	8	1,000	10	9
1,100	10	14	1,100	12	10
1,200	6	6	1,200	7	6
1,300	10	12	1,300	9	7
1,400	7	5	1,400	4	10
1,500	4	8	1,500	9	4
1,600	4	5	1,600	6	8
1,700	3	5	1,700	4	2
1,800	1	1	1,800	5	1
1,900	4	3	1,900	8	4
2,000	5	1	2,000	6	4
2,100	1	--	2,100	--	3
2,200	2	1	2,200	2	--
2,300	2	4	2,300	2	2
2,400	--	--	2,400	--	3
2,500	2	--	2,500	1	--
2,600	--	1	2,600	--	1
2,700	--	--	2,700	2	2
2,800	1	--	2,800	--	1
2,900	--	2	2,900	2	--
3,000	--	--	3,000	1	1
3,100	1	--	3,100	1	1
3,200	1	1	3,200	--	2
3,300	--	--	3,300	--	--
3,400	--	--	3,400	--	--
3,500	--	1	3,500	--	1
3,600	--	--	3,600	--	--
3,700	--	--	3,700	--	--
3,800	--	--	3,800	--	--
3,900	--	--	3,900	--	--
4,000	--	--	4,000	--	--
4,100	--	--	4,100	--	--
4,200	--	--	4,200	--	--
4,300	--	--	4,300	--	--
4,400	1	--	4,400	--	--
4,500	--	--	4,500	1	--

TABLE III

FREQUENCY DISTRIBUTION OF DERIVED GUST VELOCITY OBTAINED FROM NODAL ACCELERATIONS

Center-of-gravity position, 30.6, percent mean aerodynamic chord			Center-of-gravity position, 24.3, percent mean aerodynamic chord		
Class interval, U_{de}, fps	Frequency		Class interval, U_{de}, fps	Frequency	
	Positive	Negative		Positive	Negative
0	21	20	0	125	134
.66	87	90	.71	158	176
1.32	85	85	1.42	103	111
1.99	75	66	2.12	84	72
2.65	67	48	2.83	77	91
3.31	45	39	3.54	47	45
3.97	32	35	4.25	38	54
4.63	40	30	4.96	45	48
5.30	28	22	5.66	27	18
5.96	20	21	6.37	31	28
6.62	12	10	7.08	16	15
7.28	16	15	7.79	13	19
7.94	13	14	8.50	17	9
8.61	6	7	9.20	10	9
9.27	5	6	9.91	10	9
9.93	2	3	10.62	4	3
10.59	3	2	11.33	1	7
11.25	6	--	12.04	5	2
11.92	1	1	12.74	---	1
12.58	2	1	13.45	2	3
13.24	--	1	14.16	1	1
13.90	4	1	14.87	---	---
14.56	2	--	15.58	---	1
15.23	1	--	-----	---	---
15.89	--	--	-----	---	---
16.55	3	--	-----	---	---
17.21	1	--	-----	---	---
17.87	--	--	-----	---	---
18.54	--	1	-----	---	---

TABLE IV

STABILITY DERIVATIVES

	Center of gravity	
	Rearward	Forward
C_{Y_β}	-0.25	-0.25
C_{n_β}	0.072	0.074
C_{Y_r}	0.14	0.15
C_{n_r}	-0.052	-0.055
$\left(C_{Y_\beta}\right)_{vt}$ (for 96 sq ft only)	-0.15	-0.15
$\left(C_{Y_r}\right)_{vt}$ (for 96 sq ft only)	0.11	0.11

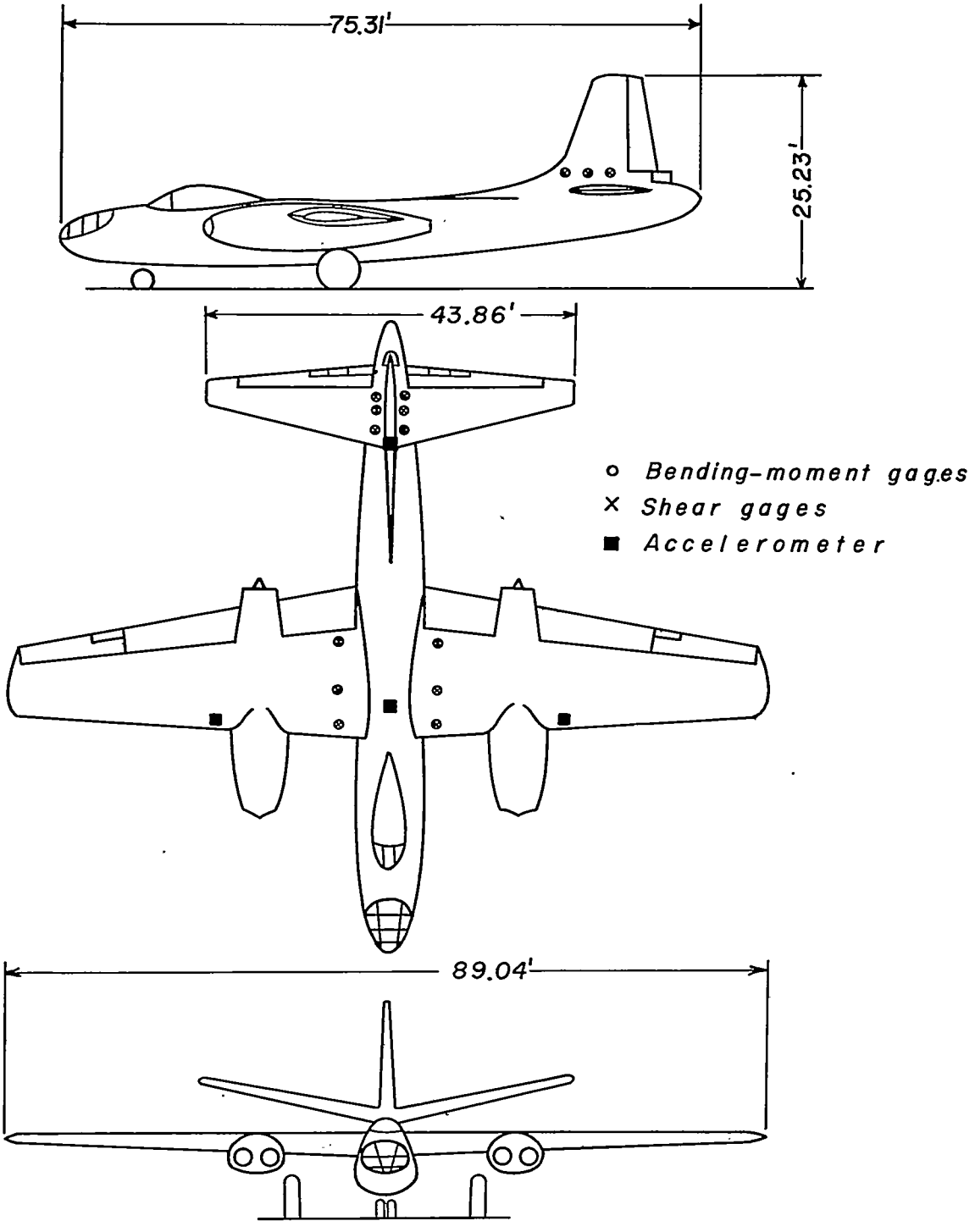

Figure 1.- Three-view drawing of test airplane.

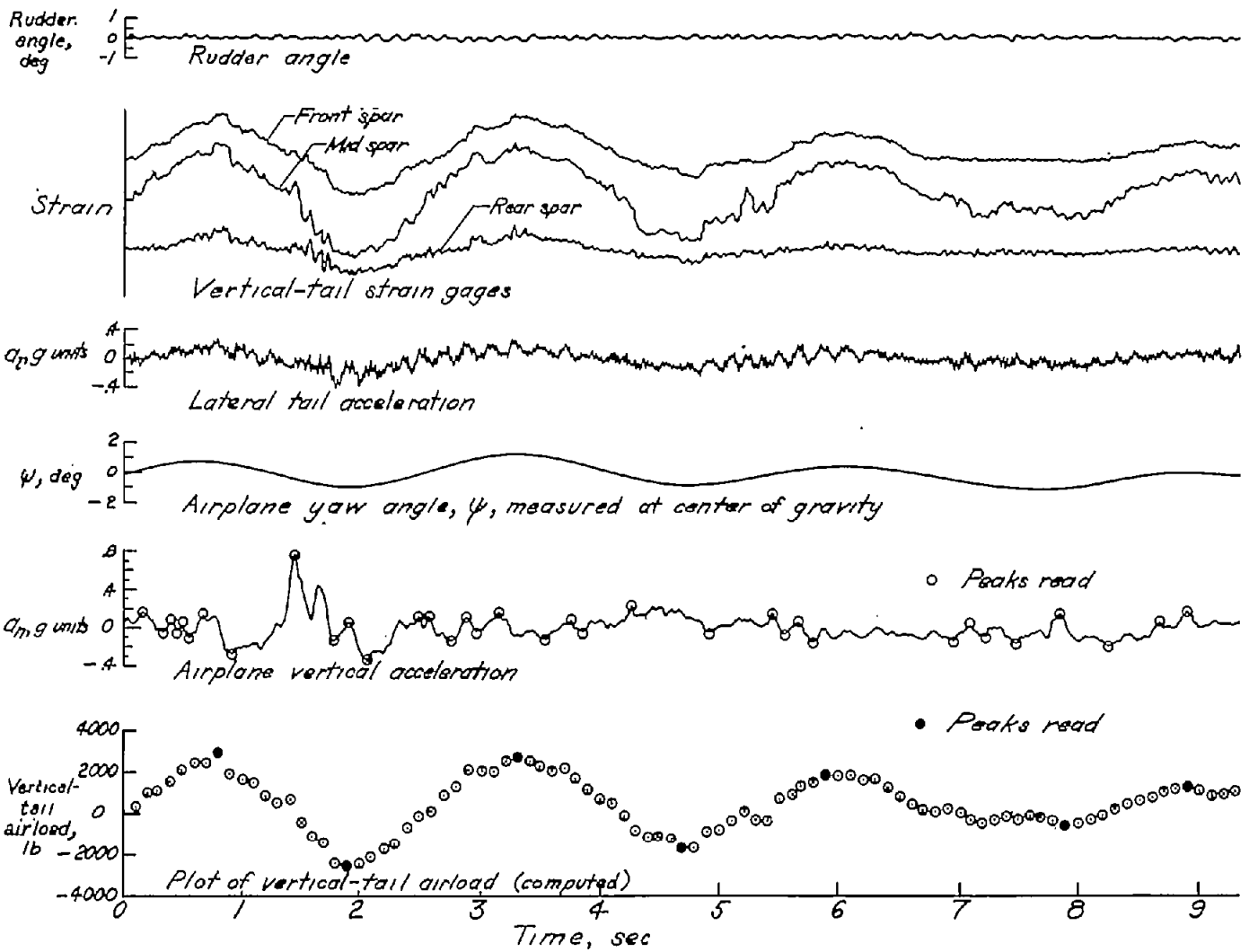

Figure 2.- Sample time histories. Airspeed, 390 knots; weight of airplane, 60,200 pounds; rearward center-of-gravity position.

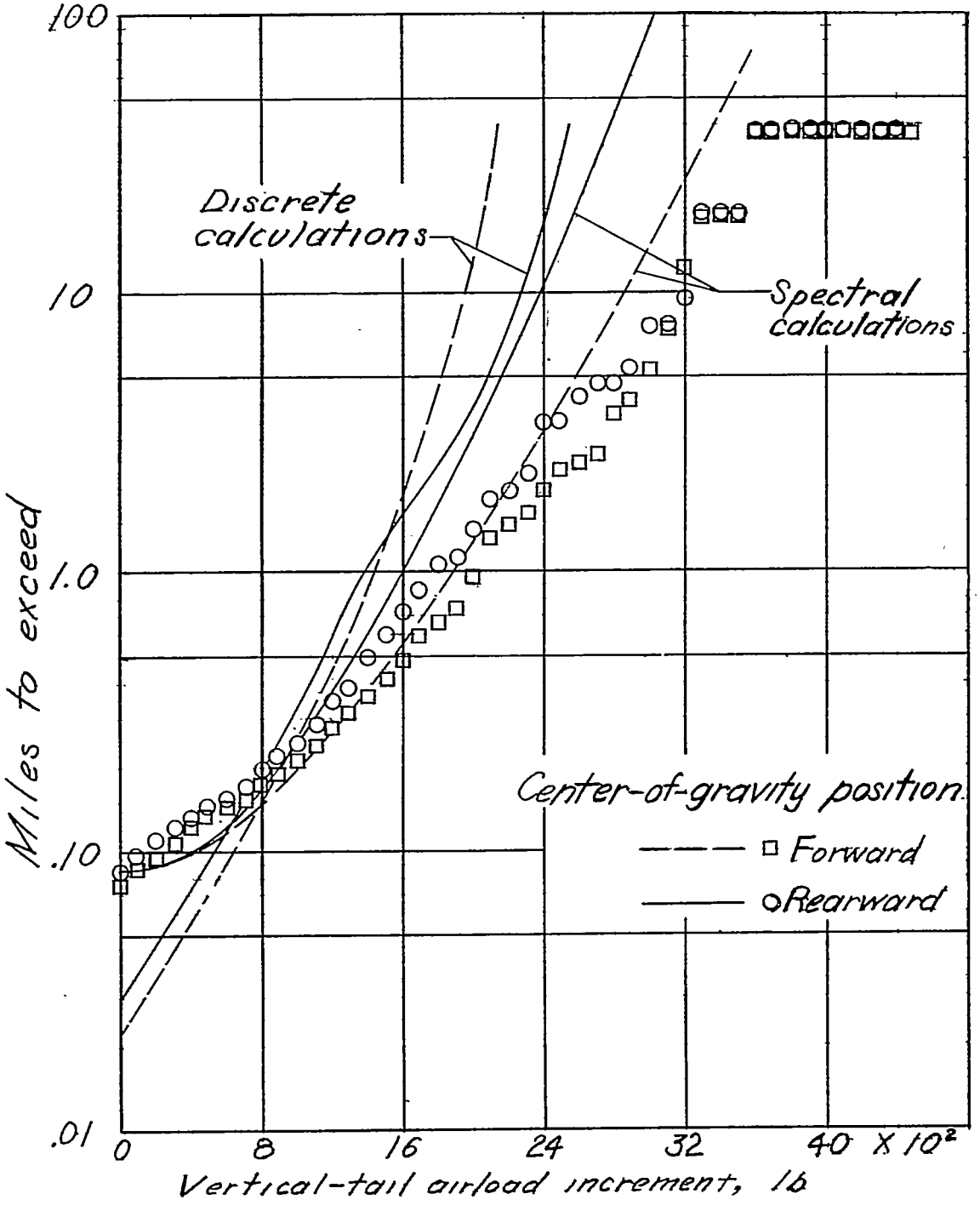

Figure 3.- Average flight miles to exceed a given load increment.

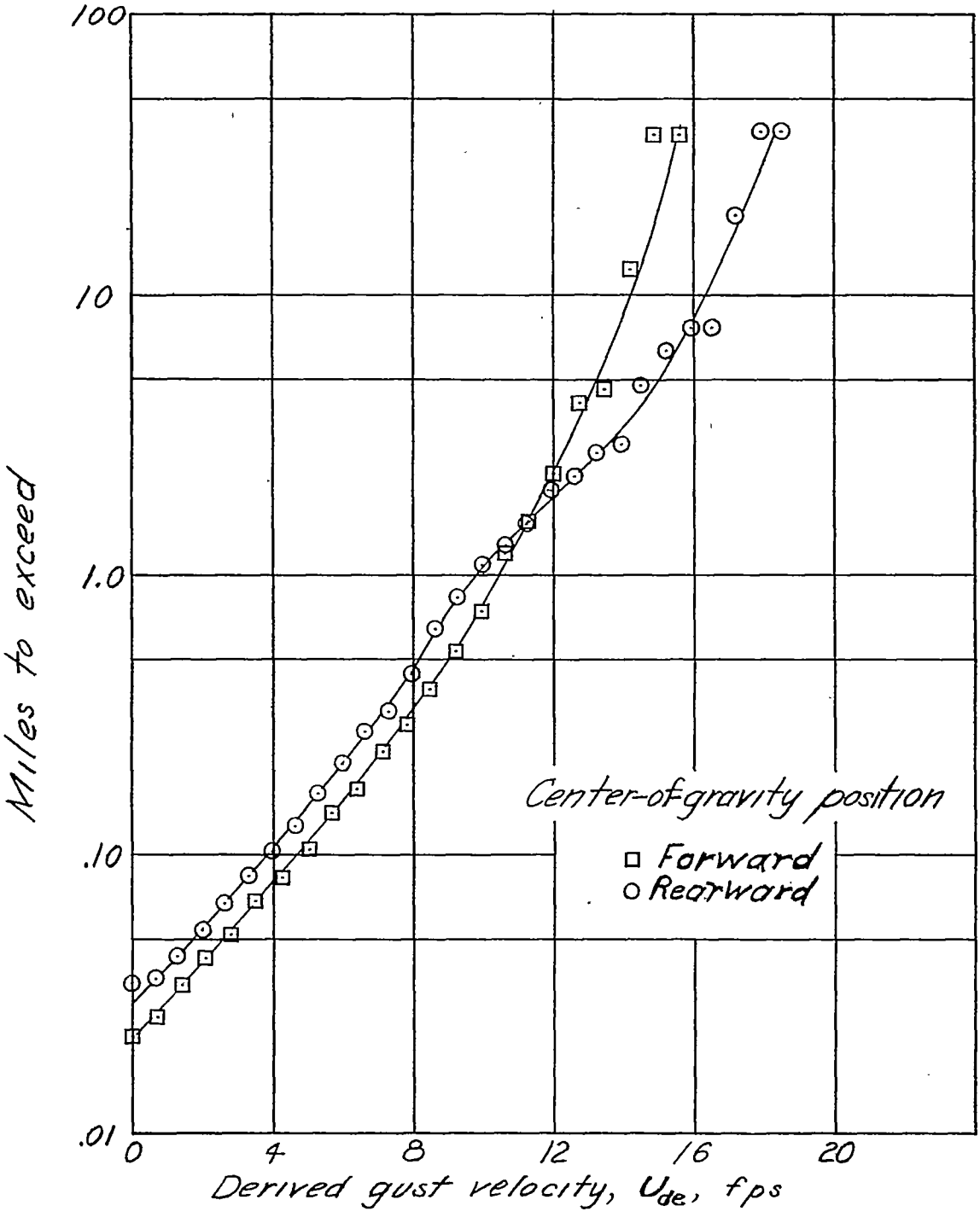

Figure 4.- Average flight miles to exceed a given derived gust velocity.

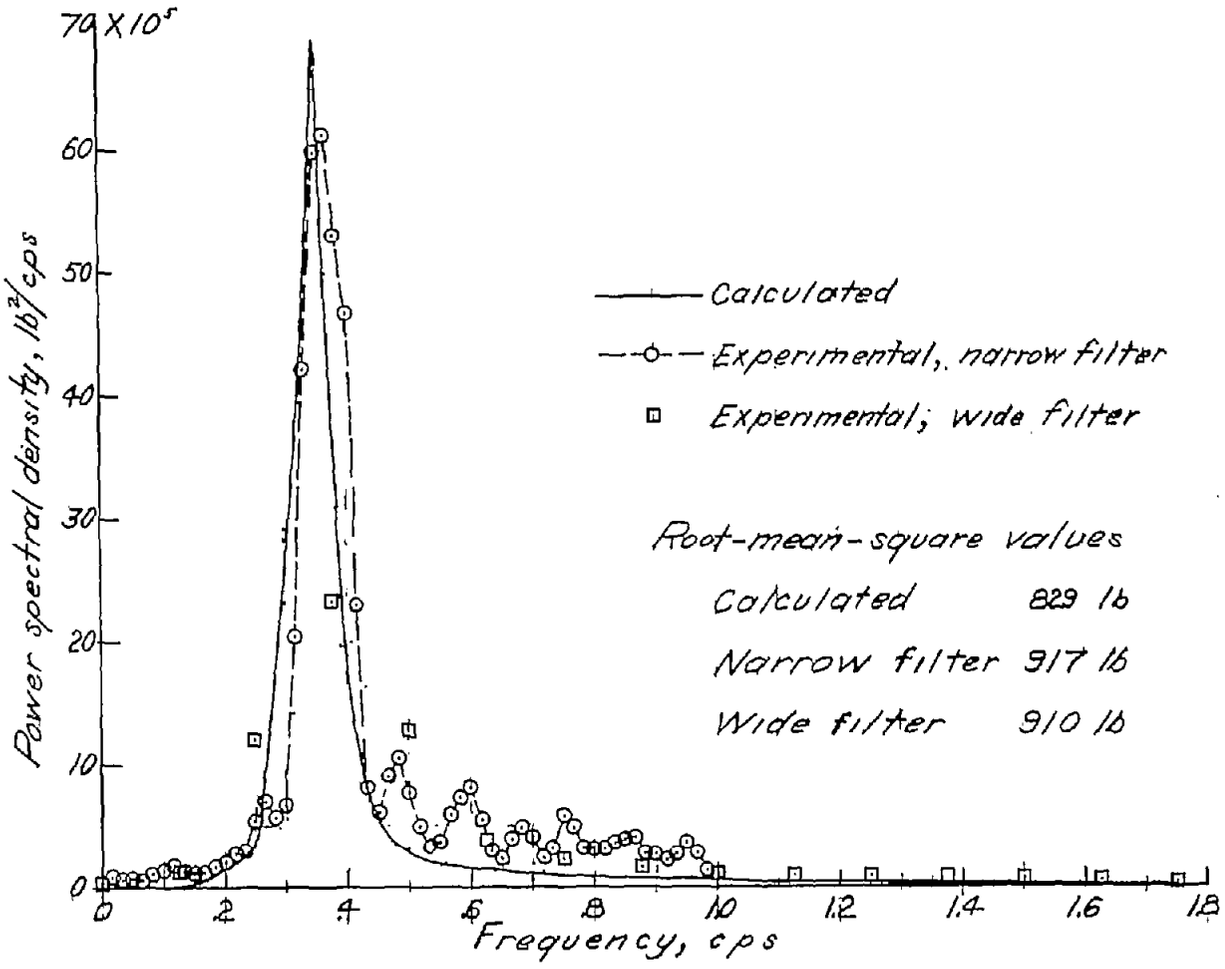

(a) Forward center-of-gravity position.

Figure 5.- Comparison of calculated and experimental power spectra of vertical-tail airload.

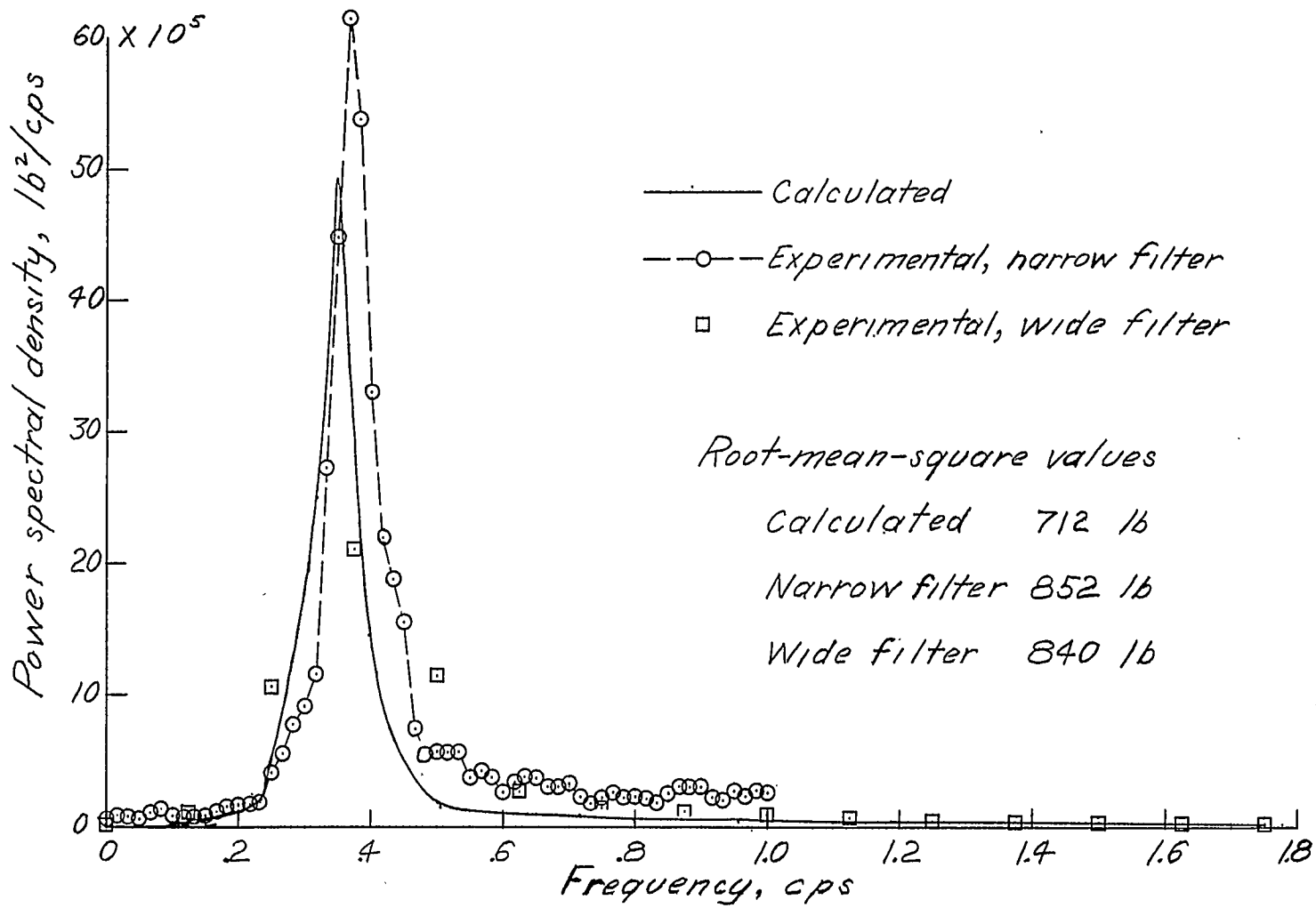

(b) Rearward center-of-gravity position.

Figure 5.- Concluded.

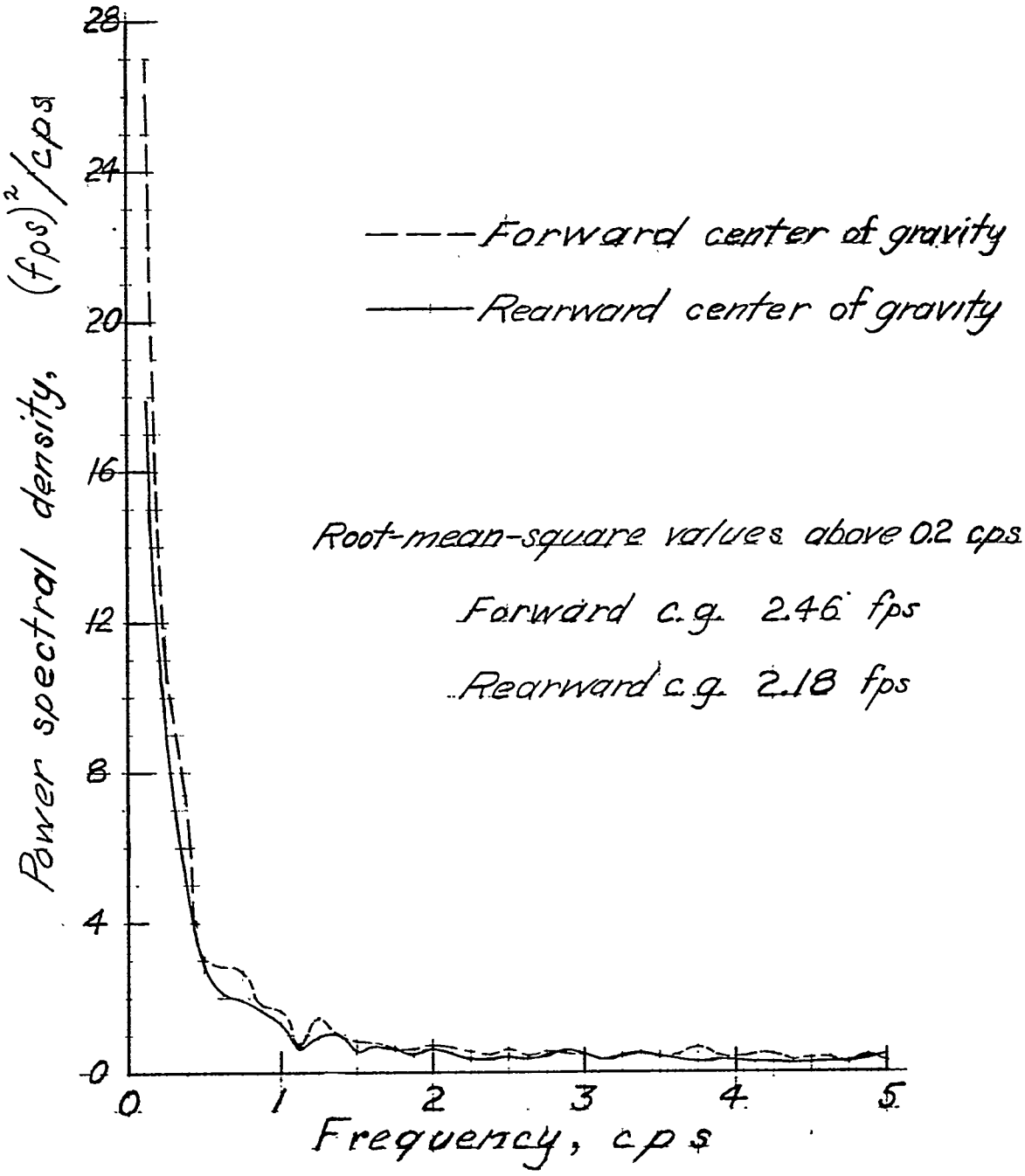

Figure 6.- Power spectra of airspeed fluctuations.

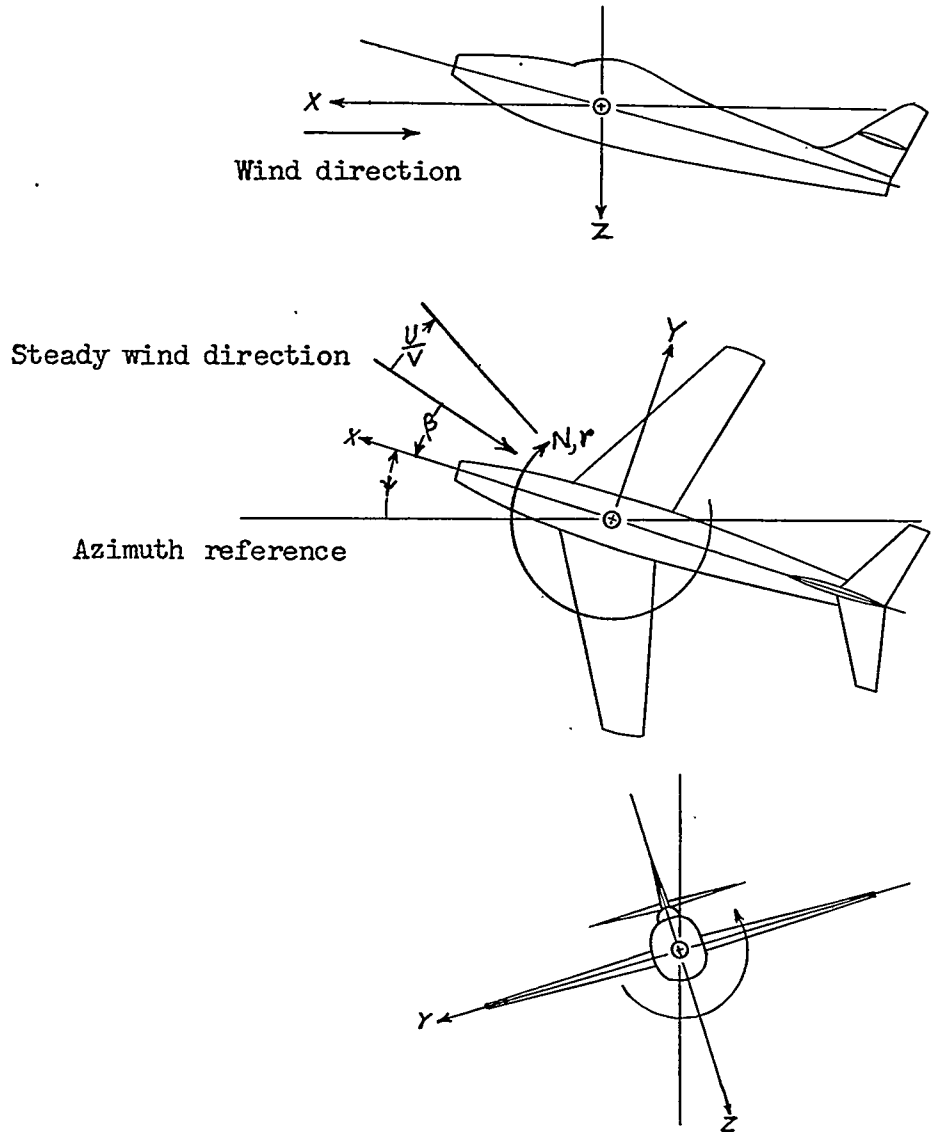

Figure 7.- Stability system of axes. Positive values of forces, moments, velocities, and angles are indicated by arrows.

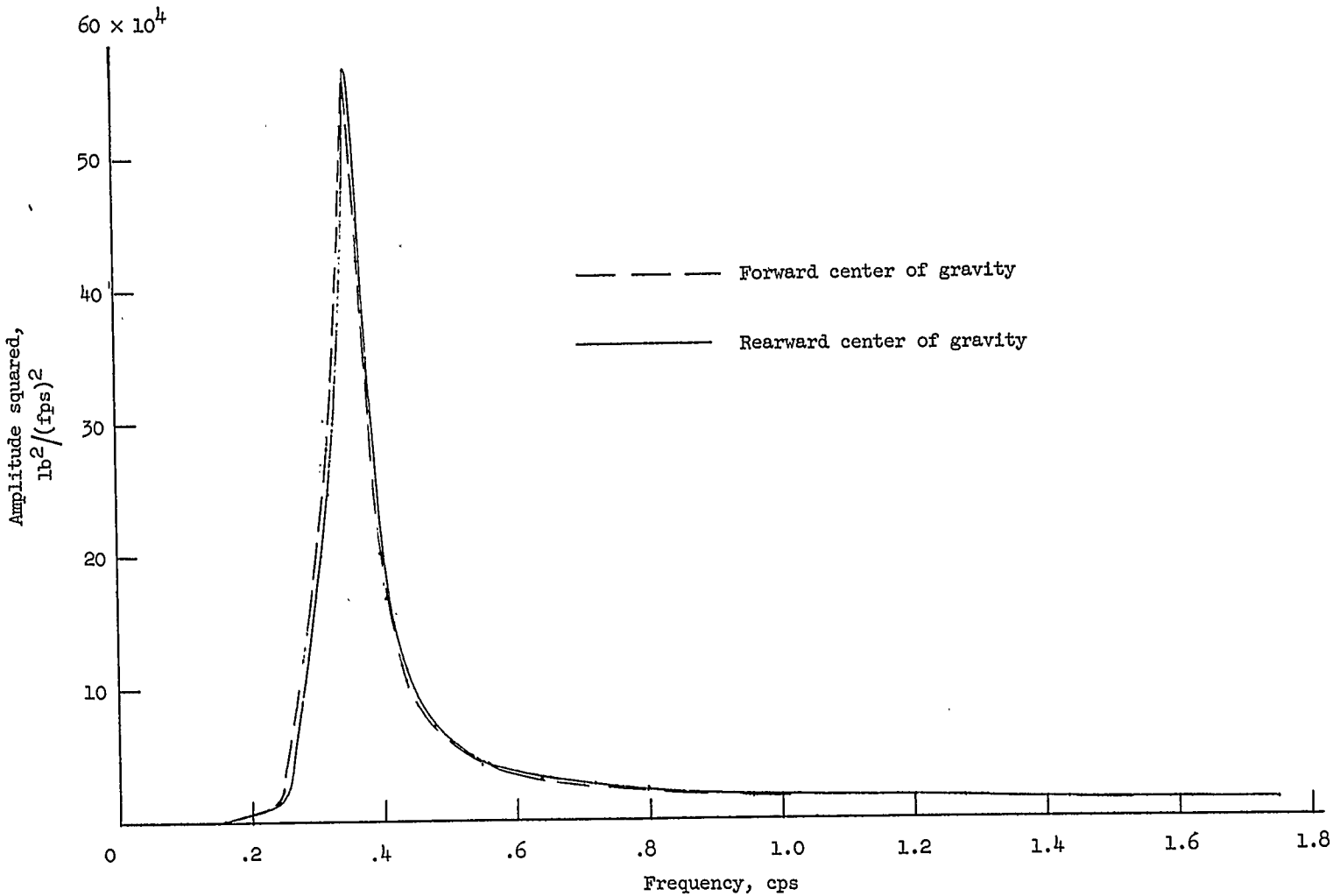

Figure 8.- Amplitude squared of calculated airplane frequency-response function for load on vertical tail.